A FIRST PRINCIPLE INVESTIGATION OF THE STRUCTURAL, MECHANICAL, AND ELECTRONIC PROPERTIES OF $NaNbO_3$ PEROVSKITE

BY

FRIDAY JOHN OLUWATOBILOBA

PSC2105508

DEPARTMENT OF PHYSICS

FACULTY OF PHYSICAL SCIENCE

UNIVERSITY OF BENIN

BENIN CITY.

NOVEMBER, 2025.

A FIRST PRINCIPLE INVESTIGATION OF THE STRUCTURAL, MECHANICAL, AND ELECTRONIC PROPERTIES OF $NaNbO_3$ PEROVSKITE

BY

FRIDAY JOHN OLUWATOBILOBA

PSC2105508

A PROJECT SUBMITTED TO THE DEPARTMENT OF PHYSICS IN PARTIAL FULFILMENT OF THE REQUIREMENT OF THE AWARD OF BACHELOR OF SCIENCE B.Sc (Hons) DEGREE IN PHYSICS

NOVEMBER, 2025.

CERTIFICATION

This is to certify that this project work titled ‘A first principle investigation on the structural, mechanical, and electronic properties of $NaNbO_3$ Perovskite’ was carried out by **FRIDAY JOHN OLUWATOBILOBA** with matriculation number **PSC2105508** in the Department of Physics, Faculty of Physical Sciences, University of Benin, Benin city.

…… ……...

Dr. M.I. BABALOLA DATE

(Project supervisor)

…… .....

PROF. C.O. AIGBOGUN DATE

(Head of Department)

…….. ……

EXTERNAL EXAMINER DATE

DEDICATION

This project work is dedicated to GOD ALMIGHTY with whom all things are possible and to my PARENTS and SIBLINGS for their endless support in my academic pursuit.

ACKNOWLEDGEMENT

I give all glory to God, the most compassionate and merciful, for the strength and opportunity to complete this project. I sincerely thank my supervisor, Dr. Babalola, for his guidance, support, and valuable ideas that made this work possible. I also appreciate my friends and lecturers in the department for their encouragement and impactful teaching. Finally, I express my heartfelt gratitude to my parents for their unwavering love and support throughout my life. This project would not have been possible without them.

ABSTRACT

This study examines the structural, mechanical, optical, and electronic properties of sodium niobate ($NaNbO_3$) perovskite using first-principles calculations within Density Functional Theory (DFT). The Generalized Gradient Approximation (GGA) and pseudopotentials in Quantum ESPRESSO were used for all computations. The optimized lattice parameters confirmed that $NaNbO_3$ crystallizes in an orthorhombic structure with space group Pbnm. The calculated elastic constants and related moduli met Born's criteria for mechanical stability. The Pugh and Poisson ratios show that the compound is near the brittle–ductile boundary. Band structure results indicate an indirect band gap of about 0.4 eV, with the valence band maximum at the Γ point and the conduction band minimum at the X point. The density of states revealed strong interaction between Nb-4d and O-2p orbitals, confirming covalent bonding within the Nb–O octahedra. These findings show that $NaNbO_3$ is a stable indirect semiconductor with potential use in optoelectronic and photovoltaic devices.

TABLE OF CONTENT

LIST OF TABLES

LIST OF FIGURES

CHAPTER ONE

INTRODUCTION

1.1 ORIGIN OF PEROVSKITE

The name **"perovskite"** comes from the mineral **$CaTiO_3$** (calcium titanate). It was first **discovered in 1839** in the Ural Mountains of Russia by the German mineralogist **Gustav Rose**. He named it **"perovskite"** in honour of the Russian mineralogist **Lev Alexeïevitch von Perovski** (1792–1856). Over time, the term perovskite was extended from just the mineral $CaTiO_3$ to a **whole family of compounds** that share the same **ABO_3 crystal structure**.

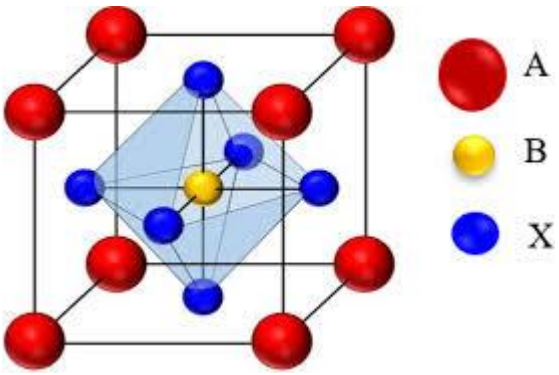

Fig 1.1: An ideal Perovskite structure

The following are the properties of perovskite:

i. they are **hard, brittle oxides**, but mechanical response depends on composition.
ii. they have a band tunability of 1–4 eV depending on cations and distortions.
iii. many are transparent wide-gap oxides ($SrTiO_3$, $NaNbO_3$).
iv. they have strong **piezoelectric** and **pyroelectric** effects in distorted phases.

The perovskite structure has the general formula **ABO_3**:

i. A-site cation: usually a large ion (e.g., Ca^{2+}, Na^{+}, Cs^{+}, or organic cations like methylammonium).

ii. B-site cation: usually a smaller transition metal ion (e.g., Ti^{4+}, Nb^{5+}, Fe^{3+}).

iii. O: oxygen anion (O^{2-}).

It is based on a **cubic or distorted cubic lattice** where the **B cation** sits in the center of an octahedron of oxygen atoms (BO_6 unit) and the **A cation** sits at the cube corners, surrounded by 12 oxygen atoms. This structure is very flexible and can accommodate different ions at A and B sites → leading to a **large family of materials** with diverse properties (ferroelectric, piezoelectric, superconducting, semiconducting, etc.).

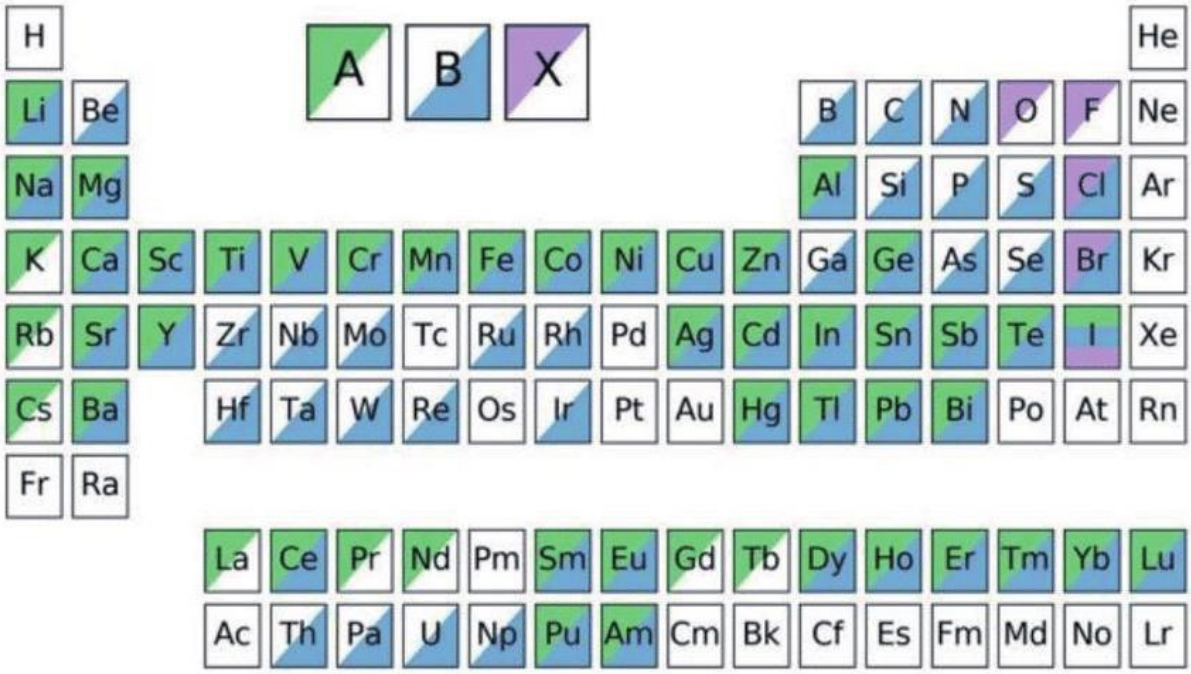

Fig. 1.2: Regions of the periodic table where A, B and X are located

1.1.1 Perovskite Compound

Perovskite compounds are a large family of materials that crystallize in the general **ABO_3 structure**, first identified in the mineral **$CaTiO_3$**. In this structure, the larger **A-site cation** (such as Na^+, Ca^{2+}, or Ba^{2+}) occupies the corners of the unit cell, while the smaller **B-site cation** (such as Ti^{4+}, Nb^{5+}, or Fe^{3+}) sits at the center of an oxygen octahedron (BO_6). The oxygen ions

are located at the face centers, completing the three-dimensional framework. This highly symmetric and flexible crystal arrangement allows for a wide variety of chemical substitutions at both A and B sites, giving rise to diverse physical and chemical properties.

The stability of perovskite compounds can be estimated using the **Goldschmidt tolerance factor (t)**, expressed as:

$$t = \frac{(rA + rO)}{[\sqrt{2}\,(rB + rO)]}$$

Where:

r_A= ionic radius of the **A-site cation**

r_B= ionic radius of the **B-site cation**

r_o= ionic radius of the **anion**

Values of *t* between 0.8 and 1.0 generally indicate stable perovskite structures. Depending on the size of the cations, perovskites can exist in **cubic, tetragonal, orthorhombic, or rhombohedral phases**, with structural distortions such as octahedral tilting influencing their properties. Because of this structural versatility, perovskite compounds exhibit a wide range of technologically relevant characteristics, including **ferroelectricity, piezoelectricity, high dielectric constants, magnetoresistance, semiconducting behaviour, superconductivity, and strong optical absorption**. For example, **$BaTiO_3$** is widely used as a ferroelectric and dielectric material in capacitors, while hybrid organic-inorganic perovskites such as **$CH_3NH_3PbI_3$** have revolutionized solar cell research due to their excellent light-harvesting efficiency.

List of notable perovskite compound

1. Calcium Titanate ($CaTiO_3$)
2. Barium Titanate ($BaTiO_3$)
3. Strontium Titanate ($SrTiO_3$)

4. Sodium Niobate ($NaNbO_3$)
5. Potassium Niobate ($KNbO_3$)
6. Lead Titanate ($PbTiO_3$)
7. Lead Zirconate Titanate ($Pb[Zr_xTi_{1-x}]O_3$, PZT)
8. Lanthanum Aluminate ($LaAlO_3$)
9. Sodium Niobate ($NaNbO_3$)

1.1.2 Double Perovskite Compound

In addition to the simple perovskite structure (ABO_3), there exists a very important class of compounds known as **double perovskites** with the general formula **$A_2BB'O_6$**. In these materials, the A-site cation remains similar to that of the simple perovskite (such as Sr^{2+}, Ba^{2+}, or Ca^{2+}), but the B-site is occupied alternately by two different cations, B and B′, instead of just one. This ordered arrangement of two different cations at the B-site introduces additional degrees of freedom in tailoring the structural, electronic, and magnetic properties of the material.

A well-known example is **Sr_2FeMoO_6**, where Fe and Mo cations alternate within the B-site lattice. This compound exhibits half-metallic ferromagnetism and has been studied extensively for spintronic applications. Similarly, **Ba_2FeReO_6** and **Sr_2CrOsO_6** show unusual magneto resistive behaviour, making them promising for magnetic sensors and memory devices.

The importance of double perovskites lies in the fact that they combine the stability and flexibility of the perovskite lattice with the tunability arising from two chemically distinct B-site cations. This allows researchers to design compounds with specific functionalities, such as high dielectric constants, multiferroic coupling, thermoelectric response, or enhanced optical

absorption. In this sense, double perovskites can be viewed as an expanded form of the simple perovskite, similar to how half-Heusler compounds are derivatives of full Heusler alloys.

1.2 Properties of Perovskite

Since perovskite materials have a unique chemical structure and stoichiometry, they have a wide range of properties, some of which are listed here:

1.2.1 Optical Properties

With single domain crystals like BaTiO3 and SrTiO3 possessing constant refractive indices across temperatures and transmitting light in the infrared spectrum, perovskite materials have optical and photoluminescence characteristics. KTN and other perovskite oxides exhibit notable electro-optic properties, which makes them valuable for laser and optical communications applications. While ecologically friendly photoluminescent materials like BaZrO3 generate light in the visible range and have potential applications in scintillators, lighting, and display technologies, rare earth-doped perovskite oxides are stable and appropriate for a variety of display technologies. (Kim et al, 2005)

1.2.2 Multiferroicity

When materials exhibit many "ferroic" properties (such as ferroelectricity, ferromagnetism, and ferroelasticity) concurrently in the same phase, this is known as multiferroicity. Often transition metal oxides with a perovskite crystal structure, such as ferrites and rare-earth manganites, are multiferroic materials that show multiferroicity even at ambient temperature. The rhombohedrally deformed perovskite bismuth ferrite is a prominent example, exhibiting both ferroelectric and antiferromagnetic ordering throughout a broad temperature range that is much higher than ambient temperature. In 2011, Singh et al. Applications in a variety of domains, including spintronics and multifunctional devices, are highly promising due to the special mix of features found in perovskite-based multiferroics.

1.2.3 Piezoelectricity

Some materials exhibit a phenomenon known as piezoelectricity, in which they produce an electrical charge in reaction to mechanical stress or deformation. On the other hand, when exposed to an external electric field, these materials can also undergo deformation or shape changes. Because piezoelectricity is bidirectional, it can be used in a number of ways. Among the synthetic piezoelectric materials are piezoelectric ceramics with a perovskite crystal structure and the general formula $A^{2+}B^{4+}O^{2-}_3$ (Aksel et al. 2011). Moreover, tendon, rochelle salt, collagen, topaz, quartz, and cane sugar are examples of natural piezoelectric materials.

1.2.4 Catalytic activity

Because of their remarkable catalytic activity and great chemical stability, perovskites can be used to catalyze changed processes. They function as active site models and fall into one of two categories: oxidation or oxygen-activated catalysts. Roni (2018)

1.2.5 Superconductivity

When materials cool significantly, magnetic flux fields are released as their electrical resistance falls to zero, a phenomenon known as superconductivity. A good framework for obtaining superconductivity is provided by the crystal structure of perovskite oxides. Copper-containing perovskites hold great promise as high-temperature superconductors. La-Ba-Cu-O perovskite was the first example. In contrast to intermetallic compounds such as cesium tungsten bronzes, perovskite oxides have emerged as a more common source of superconductors. Cava (2008).

1.3 Applications of Perovskite

Perovskite materials are used in many modern technologies because of their unique properties and flexible structure. They play important roles in solar cells, LEDs, photodetectors, dielectric and ferroelectric devices, as well as in catalysis and fuel cells.

1.3.1 Perovskite Solar Cells (PSCs)

Materials such as methylammonium lead iodide ($MAPbI_3$) act as the light-absorbing layer in perovskite solar cells. When exposed to sunlight, they generate electron-hole pairs that move through charge-selective layers to produce electricity.

Key advantages:

i. High Power Conversion Efficiency above 25%, comparable to silicon solar cells.
ii. Low production cost using simple solution-based methods.
iii. Flexible and lightweight, ideal for portable and wearable electronics.
iv. Adjustable bandgap, allowing combination with silicon cells for better efficiency.

1.3.2 Perovskite Light-Emitting Diodes (PeLEDs)

In PeLEDs, electrons and holes are injected into a perovskite layer where they recombine to emit light. Their narrow emission spectrum and strong luminescence make them promising for display and lighting applications.

Key advantages:

i. High efficiency, comparable to OLEDs and QLEDs.
ii. Tunable emission from ultraviolet to near-infrared by adjusting halide composition.
iii. High color purity with vivid, well-defined output.

1.3.3 Perovskite-Based Photodetectors

Perovskite photodetectors convert light into electrical signals for use in imaging and sensing. Their strong light absorption and long carrier diffusion length make them efficient. Key advantages:

i. Wide spectral response from ultraviolet to near-infrared.

ii. High sensitivity with low noise and strong signal detection.

iii. Easy and affordable production using solution processes.

1.3.4 Perovskite Dielectrics and Ferroelectric Devices

Perovskites like $BaTiO_3$ and $PbTiO_3$ show strong dielectric and ferroelectric behavior. These features are useful in capacitors, memory devices, and tunable microwave components. Key advantages:

i. High dielectric constant for effective energy storage.

ii. Ferroelectric switching used in non-volatile FeRAM memory.

iii. Adjustable microwave properties for communication systems.

1.3.5 Perovskite Catalysis and Fuel Cells

Compounds such as $La_{0.6}Sr_{0.4}MnO_3$ and $LaFeO_3$ are used as electrodes in solid oxide fuel cells and as catalysts for oxygen reduction and evolution reactions. Their thermal stability and oxygen ion conductivity make them efficient for energy conversion. Key advantages:

i. Strong oxygen ion conductivity enhances electrochemical reactions.

ii. Lower cost compared to platinum-based catalysts.

iii. Stable performance under high temperatures for long-term fuel cell use.

1.4 AIM AND OBJECTIVES

AIM

The aim of the study is to investigate the structural, mechanical, optical, and electronic properties of $NaNbO_3$ using first-principles calculations.

OBJECTIVES

The objectives of this study are to;

1. determine the optimized structural parameters of $NaNbO_3$ using Density Functional Theory.
2. analyse the mechanical stability and elastic properties of $NaNbO_3$.
3. examine the optical and electronic properties of $NaNbO_3$ for potential device applications.

CHAPTER TWO

2.1 Literature Review

Perovskite oxides with the general formula ABO_3 are fundamental in solid-state physics and materials science because of their flexible structure and wide range of physical behaviors. Their lattice allows the substitution of various cations, enabling precise tuning of distortions, band structures, and functional responses. Among these compounds, niobate-based perovskites (A–Nb–O, where A = Li, Na, K, Rb, or Cs) are widely recognized for their ferroelectric, piezoelectric, and nonlinear optical properties. They are important for modern applications such as capacitors, sensors, non-volatile memory devices, and optical modulators. Sodium niobate ($NaNbO_3$), in particular, has attracted significant interest due to its complex phase behaviour and promising electronic and electromechanical properties compared with its well-known analogs $KNbO_3$ and $LiNbO_3$.

The ideal cubic perovskite structure (space group $Pm\bar{3}m$) consists of corner-sharing NbO_6 octahedra, with Na^+ ions occupying the 12-fold coordinated A-site. Structural deviations from this symmetry occur mainly due to ionic size mismatch, which is expressed through the Goldschmidt tolerance factor,

$$t = (r_A + r_O)/\sqrt{2}(r_B + r_O) \quad \text{..... (2.1)}$$

When t differs from unity, distortions arise, leading to orthorhombic, rhombohedral, or tetragonal structures that often exhibit ferroelectric displacements and octahedral tilting (Mitchell, 2002).

For $NaNbO_3$, the ionic radius of Na^+ (1.02 Å) yields a tolerance factor close to 1, suggesting the possibility of a nearly cubic or slightly distorted perovskite framework.

Despite this, $NaNbO_3$ does not retain a cubic perovskite structure at ambient conditions. Nelmes et al. (1980) reported that the compound stabilizes in an orthorhombic antiferroelectric phase under standard pressure. High-pressure synthesis studies, such as those by Yamamoto et

al. (2024), have shown that alkali niobates can transition into dense perovskite-type structures at elevated pressure and temperature. For example, the formation of high-pressure phases in similar niobates reveals significant volume reduction and orthorhombic distortion, which tend to revert to lower-symmetry forms at ambient pressure. Such behavior highlights the importance of computational modeling through first-principles Density Functional Theory (DFT), which provides detailed insight into the structural stability, phonon dynamics, and electronic behavior of $NaNbO_3$ under varying thermodynamic conditions.

2.2 Density Functional Theory (DFT) Investigations

2.2.1 Structural and Energetic Stability

Lebedev (2015) performed one of the most detailed first-principles analyses of $NaNbO_3$ using both the Local Density Approximation (LDA) and Generalized Gradient Approximation (GGA). Phonon dispersion studies on the cubic $Pm\bar{3}m$ phase showed imaginary frequencies at the Γ and R points, indicating dynamic instability. When these unstable modes condensed, lower-symmetry phases such as rhombohedral (R3m), tetragonal (P4mm), and orthorhombic (Amm2) emerged. The rhombohedral R3m structure was identified as the lowest-energy configuration at ambient conditions. The calculated lattice constants were 4.09 Å (LDA) and 4.15 Å (GGA-PBE), with a rhombohedral distortion angle near 89.5°, reflecting a ferroelectric displacement of Nb relative to O atoms. The computed spontaneous polarization of 0.46 C/m^2 was higher than in $KNbO_3$ (0.37 C/m^2) and $BaTiO_3$ (0.26 C/m^2), confirming strong ferroelectric character in $NaNbO_3$.

2.2.2 Phonon and Vibrational Properties

Phonon analysis provides critical insight into perovskite stability. In cubic $NaNbO_3$, soft phonon modes with imaginary frequencies near 90i cm^{-1} were identified at the Γ point, linked to ferroelectric instabilities leading to the R3m phase. The phonon density of states revealed

strong Nb 4d–O 2p coupling in the 500–800 cm^{-1} region, indicating partial covalency in Nb–O bonds. Similar behavior has been observed in $KNbO_3$ and $CsNbO_3$, suggesting that soft-mode phonon instabilities are intrinsic to the A–Nb–O series. **Phonon dispersion** shows no imaginary frequencies, confirming **structural stability**.

2.2.3 Mechanical Properties

Sharma and Singh (2019) computed the elastic constants for the R3m phase of $NaNbO_3$ using GGA-PBEsol: C_{11} = 4052.07 GPa, C_{12} = 724.77 GPa, C_{44} =741.44 GPa, and. These values satisfy Born's stability conditions. The derived moduli were B = 143 GPa, G = 1031.47 kbar, and E = 2603.83 kbar, yielding a Pugh ratio of 1.88, which places the compound at the ductile–brittle transition. The Poisson's ratio of about 0.29 indicates mixed ionic–covalent bonding. Increasing pressure strengthens the lattice and suppresses ferroelectric distortion, consistent with experimental observations in high-pressure studies.

2.2.4 Electronic Structure and Band Gap

$NaNbO_3$ is a wide-band-gap semiconductor with a direct gap at the Γ point. LDA predicts 2.32 eV, GGA-PBE gives 2.68 eV, and advanced methods like HSE06 and GW yield 3.4–3.6 eV. The valence band is dominated by O 2p orbitals, while the conduction band mainly involves Nb 4d orbitals, indicating d–p charge-transfer characteristics. Na contributes minimally near the Fermi level and acts primarily as a charge-balancing cation. The wide band gap implies strong optical transparency, making $NaNbO_3$ suitable for optoelectronic and photoferroelectric devices. The calculated Born effective charges, $Z^*(Nb) = +8.7$ e and $Z^*(O\|) = -6.6$ e, confirm pronounced dynamic charge transfer and strong ferroelectric polarization.

2.2.5 Optical and Dielectric Properties

Hybrid-functional DFT calculations predict a static dielectric constant of about 31 and a refractive index of 2.45 at 550 nm. The absorption edge appears near 3.4 eV, with major peaks

between 5.5 and 6.0 eV due to Nb–O charge-transfer transitions. The predicted piezoelectric coefficient, $d_{33} \approx 47$ pC/N, is comparable to $KNbO_3$ (45 pC/N) and $BaTiO_3$ (51 pC/N), confirming strong electromechanical coupling. These results support the potential use of $NaNbO_3$ in piezoelectric sensors and optical applications.

2.2.6 Comparative Trends across Alkali Niobates

Across the A–Nb–O series, increasing A-site ionic radius (Li → Cs) decreases polarization strength and lattice distortion. $NaNbO_3$, with an intermediate cation size, lies near the boundary between ferroelectric and antiferroelectric behavior. The calculated energy difference between the polar (R3m) and nonpolar ($Pm\bar{3}m$) phases is about 109 meV per formula unit, smaller than in $KNbO_3$ (153 meV) but larger than in $CsNbO_3$ (57 meV). This explains its pressure-sensitive ferroelectricity, where modest compression suppresses polarization above roughly 3 GPa. Mechanical stiffness follows a similar chemical trend, confirming that the A-site size strongly influences both elasticity and polarization.

2.2.7 Computational Methodology

Reliable DFT modeling requires appropriate exchange–correlation functional selection. LDA tends to underestimate lattice constants, GGA slightly overestimates them, and PBEsol offers balanced accuracy. Hybrid (HSE06) and GW methods improve band-gap predictions. Phonon properties are computed via Density Functional Perturbation Theory (DFPT) to identify unstable modes linked to ferroelectric transitions. Elastic constants are derived from stress–strain relationships, and Born's criteria ensure mechanical stability: $C_{11} - |C_{12}| > 0$, $(C_{11} + 2C_{12})C_{33} - 2C_{13}^2 > 0$, and $C_{44} > 0$.

All tests confirm the mechanical and structural stability of $NaNbO_3$ across its stable pressure range.

2.2.8 Research Gaps and Prospects

Although computational research on $NaNbO_3$ has advanced, several areas remain underexplored. The temperature-dependent phase transitions and elastic responses under varying pressure are not fully characterized. Limited optical studies using hybrid or GW methods exist, and the role of point defects such as oxygen vacancies or Na deficiencies has not been adequately examined. These defects likely influence conductivity, polarization switching, and long-term material stability. Addressing these gaps through combined experimental and first-principles approaches will enhance understanding of how structural, electronic, and mechanical factors interact in $NaNbO_3$, supporting the development of reliable perovskite materials for advanced optoelectronic and energy applications.

CHAPTER THREE

METHODOLOGY

3.1 DENSITY FUNCTIONAL THEORY (DFT)

Density functional theory (DFT) is a quantum-mechanical atomistic simulation method to compute a wide variety of properties of almost any kind of atomic system: molecules, crystals, surfaces and even electronic devices when combined with non- equilibrium Green's functions (NEGF). DFT belongs to the family of first principles (ab initio) methods, so named because they can predict material properties for unknown systems without any experimental input (Meg, et al 2007). DFT has been established as a valuable research tool because it can serve either to validate the conclusions that have been reached from the analysis of the experiments or to distinguish between those possibilities that were left open. The calculation of a wide range of molecular properties with DFT allows a close connection between theory and experiment and often leads to important clues about the geometric, electronic, and spectroscopic properties of the systems being studied. DFT appears generally reliable for geometries, vibrational frequencies, and total energies, having over wavefunction based methods the advantage of quick convergence to the basis set limit Hohenberg and Kohn (1964). DFT appears to be quite successful for the prediction of molecular properties as well, since a number of spectroscopic properties of interest to the bioinorganic community can be predicted with good accuracy. DFT is formulated for zero K calculations, i.e., without lattice vibrations. Finite temperature effects can be modelled either by ab initio molecular dynamics, in which the forces acting on each atom of the system are calculated from first-principles calculations and the temperature is controlled by a thermostat rescaling the atom velocities, or by the calculation of the phonon spectrum of the material.

To get a first idea of what density-functional theory is about, it is useful to take a step back and recall some elementary quantum mechanics. In quantum mechanics, we learnt that all information we can possibly have about a given system is contained in the system's wave function Ψ. The Schrodinger equation for calculating the ground state energy of a collection of atoms in the time independent, non-relativistic approach is given as:

$H\Psi(x_1, x_2, ..., x_n) = E\Psi(x_1, x_2, ..., x_n)$ ..... (3.1)

where H is the Hamiltonian operator, $\Psi(x_1, x_2, ..., x_n)$ is a wave function written with space-spin coordinates $x_i = (r_i, \sigma_i)$ which is antisymmetric with respect to the exchange of two coordinates, and E is the associated energy.

3.2 THE GENERALIZED GRADIENT APPROXIMATION (GGA)

Generalized Gradient Approximations (GGA) to the exchange correlation (XC) energy in density functional theory are currently receiving growing interest as a simple alternative to improve over the local density approximation (LDA) in ab initio total-Energy calculations (Marvin, et al., 1989). The accuracy of LDA is often considered satisfactory in condensed matter systems, but it is much less se in atomic and molecular physics, for which highly accurate experimental data are available. Also, LDA overestimates (-20% and more), Cohesive energies and bond strengths in molecules and solids, and as a consequence bond length are often underestimated. Such problems are mostly corrected by the introduction of gradient corrections. The exchange-correlation functional is written as a function of the local density and of the local gradient of density. Also, as the LDA approximate the energy of true density by the energy of a local constant density, it fails in the situation where the density undergoes rapid changes such as in molecules. The first logical step to go beyond LDA is the use of not only the information about the density of electron, n(r) at a point, but also to supplement the density with information about the gradient of density, n(r) in order to account for non-homogeneity of the true electron density. These are two set of functional forms widely used in

Exchange Correlation Energy. introduced respectively by Perdew and Wang in 1992 and Perdew, Burke and Enzerhof in 1996 (PBE). It is observed that GGA in PBE form give rather accurate results for most of the periodic systems. Both LDA and GGA perform badly in materials where the electrons tend to be localized and strongly correlated such as transition metal oxides and rare earth elements and compounds. This drawback leads to approximations beyond LDA and GGA.

The GGA is a variant of the generic type and is represented as:

$E_xc^{GGA}[n] = \int n(r)\varepsilon_xc^{GGA}[n(r), \Delta n(r)]d^3r$ ..... (3.2)

In pseudopotential calculations, the total energy is formally treated as a functional of the valence charge density alone with the pseudopotentials accounting for the interaction of the valence electrons with the nuclei and with the core electrons namely, for Pauli repulsion, electrostatic and XV interactions to within the frozen core approximation. Substituting the GGA for the LDA modifies the treatment not only of the XC interactions of the valence electrons among themselves but also that of the core-valence (CV) interactions. According to Perdew-Wang (1991), within the pseudopotential framework the GGA total-energy functional reads

$E^{GGA}_{tot}[n] = T_0[n] + E_h[n] + E_xc^{GGA}[n] + \sum_i^{Occ} \langle\Psi_i|V^{GGA}/\Psi_i\rangle$ (3.3)

Where the various terms denote the non-interacting kinetic energy, the Hartree energy, the XC energy and the potential energy of the valence electrons, represented by the pseudo-wave functions (r) and the corresponding charge density $n(r) = \sum_i^{Occ} |\Psi(r)|^2$ in the presence of the ion cores, represented by GGA pseudopotentials, V^{GGA}. The LDA counterpart is obtained by substituting the XC energy E_xc^{LDA} and the LDA pseudopotential V^{GGA} for the respective GGA entities.

however, significantly fails in the description of many properties of d and f compounds. Binding energies are in particular overestimated. For most materials, GGA improves the LDA

over binding. The failure of standard LDA and GGA is generally attributed to the use of a local potential to treat exchange or to the inadequate treatment of the many-body electron correlations. However, both GGA and LDA approximations are known to underestimate the band gap of semiconductors by about 30 to 80% and to inaccurately describe the band structure of strongly correlated materials.

3.4 PSEUDOPOTENTIALS AND APPLICATIONS

One of the main advantages of using a plane wave basis set is that its accuracy can be easily controlled. This is related to the fact that, when using such a basis set, we are making no assumptions about the final shape of the orbitals, other than that there is some scale below which they become smoothly varying (Sverre, 2011).

However, this also leads to a major disadvantage of using a plane wave basis set, which is that the size of the basis set required for a given system is often far larger than would be required with a localized basis set. This is because in condensed matter systems, the orbitals tend to oscillate very rapidly in the vicinity of atomic nuclei, and are much more smoothly varying elsewhere. In order to describe this rapid oscillation, we must set very large cut-off energy, so that we include plane wave with very short wavelengths. But, since most of the space in the cell does not contain rapidly oscillating orbitals, most of the computational expenses associated with all this plane waves effectively goes to waste. A localized basis set can be tailored such that the basic functions themselves are rapidly oscillating in the vicinity of atomic nuclei and more smoothly oscillating elsewhere, so that the total number of basic functions required for the system is far smaller (Louie, 1982). The use of pseudopotential, in conjunction with plane waves, can dramatically reduce the magnitude of this problem. To understand what pseudopotential does, we note the following two facts orbitals in condensed matter system. i. Lower energy orbitals can often be considered to represent core electrons. These are electrons that are well localized around an atomic nucleus and whose properties do not change

significantly with the atom's chemical environment. ii. Orbitals representing electrons that are not core electrons oscillate very rapidly in the vicinity of atomic nuclei but most of this oscillation can be put down to the fact that they have to be orthogonal to the core electrons. A pseudopotential essentially changes part of what the outer or valence, electron "see". The core electrons and the potential due to the bare nuclear charge are replaced by a fictious potential that is defined such that the behaviour of the valence electrons is not affected outside of some cut-off radius from the nucleus. So long as this radius is not large that it overlaps regions of space that are involved in chemical bonding, the pseudopotential approximation should not significantly alter the interatomic interactions that govern the behaviour of condensed matter. Using pseudopotentials reduces the computational cost of a calculation in three ways;

a) By effectively removing core electrons from the calculation, the number of Kohn-Sham orbitals is reduced. This reduces the memory required to store the orbitals, the time required to evaluate orbital dependent quantities and the time required to normalize a set of orbitals.

b) Because there are no core-electrons to which valence electrons must be orthogonal, there is less oscillation of the corresponding orbitals in the vicinity of the nucleus. This means that lower cut-off energy can be used to represent the orbitals, resulting in lower memory requirements and greater speed. This lowering of the cut-off energy is typically a few orders of magnitude resulting in massive gains in efficiency.

c) Because the pseudopotential is not uniquely defined for a particular element, we can optimize the shape of the potential so as to give as low a required cut- off energy as possible. Again, this reduces memory and increases speed. Because we only explicitly treat the valence electrons in a calculation when using pseudopotentials, we tend to think of the system as being made of electrons and ions rather than electrons and nuclei.

3.4.1 Quantum Espresso

QUANTUM ESPRESSO is an integrated suite of computer codes for electronic- structure calculations and materials modelling based on density-functional theory, plane waves basis sets and pseudopotentials to represent electron-ion interactions. QUANTUM ESPRESSO is free, open-source software distributed under the terms of the GNU General Public License (GPL). ESPRESSO is an acronym for open-source package for research in electronic structure, simulation and optimization. The QUANTUM ESPRESSO distribution is written, mostly, in Fortran-95, with some parts in C or in Fortran-77. It implements a variety of methods and algorithms aimed at a chemically realistic modelling of materials from the nanoscale upwards, based on the solution of the density-functional theory (DFT) problem, using a plane waves (PW) basis set and pseudopotentials to represent electron-ion interactions. The codes are constructed around the use of periodic boundary conditions, which allows for a straightforward treatment of infinite crystalline systems, and an efficient convergence to the thermodynamic limit for a periodic but extended systems, such as liquids or amorphous materials (Baroni, et al 2009). Finite systems are also treated using supercells; if required, open-boundary conditions can be used through the use of the density-counter charge method. Codes in the package are based on density functional theory and on a plane wave/pseudopotential description of the electronic ground state and are ideally suited for structural optimizations (both at zero and at finite temperature), linear response calculations (phonons, elastic constants, dielectric and Raman tensors, etc.) and high temperature molecular dynamics. QUANTUM ESPRESSO can thus be used for any crystal structure or supercell, and for metals as well as for insulators (Corso,et al 1990). The core plane wave DFT functions of Quantum Espresso are provided by the PWscf component. PWscf (Plane-Wave Self-Consistent Field) is a set of programs for electronic structure calculations within density functional theory and density functional perturbation theory, using plane wave basis sets and pseudopotentials.

3.4.2 What Quantum Espresso can do

Quantum espresso can be used to perform the following task:

i. Ground state calculations utilizing local density approximation (LDA), Generalized Gradient Approximation (GGA), GGA+U, van der Waals (vdW-DF) and Hybrid Exchange-Correlation Functional.
ii. Structural optimization and polymorphism studies
iii. Transition states and minimum energy paths using Nudged Elastic Bands (NEB) method
iv. Linear response properties within Density Functional Perturbation theory (DFPT)
v. Spectroscopic properties
vi. Quantum import
vii. Ab initio Molecular Dynamics
viii. Generation of pseudopotentials

The following shell scripts were used to optimize the parameters;

Create 1.sh

```
#!/bin/sh
sys='nanbo3'
for CUTOFF in 30 35 40 45 50 55 60 65 70 75 80
do
cat > $sys.scf.in << EOF
&CONTROL
   calculation = 'scf'
   prefix = 'NaNbO3',
   outdir = './',
```

```
   pseudo_dir = '/home/john/PSEUDOPOTENTIALS',
   /
&SYSTEM
   ibrav = 1,
   celldm(1) = 7.419,
   nat = 5,
   ntyp = 3,
   ecutwfc = $CUTOFF,
   occupations = 'smearing',
   smearing = 'mp',
   degauss = 0.02,
   nspin = 1,
/
&ELECTRONS
   conv_thr = 1.0d-8,
   mixing_beta = 0.7,
   diagonalization = 'david',
/
ATOMIC_SPECIES
   Na   22.9898  Na.pbe-spn-kjpaw_psl.0.2.UPF
   Nb   92.9064  Nb.pbe-spn-kjpaw_psl.0.3.0.UPF
   O    15.9994  O.pbe-n-kjpaw_psl.1.0.0.UPF
```

```
ATOMIC_POSITIONS {crystal}
   Na  0.0  0.0  0.0
   Nb  0.5  0.5  0.5
   O   0.5  0.0  0.5
   O   0.0  0.5  0.5
   O   0.5  0.5  0.0

K_POINTS {automatic}
   6 6 6 0 0 0
EOF
  mpirun --oversubscribe -np 4 ~/qe-6.7/bin/pw.x < $sys.scf.in > $sys.scf.out
awk '/kinetic/{alat=$(NF-1)}/!/{print alat, $(NF-1)}' $sys.scf.out >> ecut
 done
```

Create 2.sh

```
#!/bin/sh
sys='nanbo3'
for alat in 3 4 5 6 7 8 9 10 11
do

# self-consistent calculation
cat > $sys.scf.in << EOF
&CONTROL
   calculation = 'scf'
   prefix = 'NaNbO3',
```

```
    outdir = './',
    pseudo_dir = '/home/john/PSEUDOPOTENTIALS',
    /
&SYSTEM
    ibrav = 1,
    celldm(1) = 7.689,
    nat = 5,
    ntyp = 3,
    ecutwfc = 75,
    occupations = 'smearing',
    smearing = 'mp',
    degauss = 0.02,
    nspin = 1,
/
&ELECTRONS
    conv_thr = 1.0d-8,
    mixing_beta = 0.7,
    diagonalization = 'david',
/
ATOMIC_SPECIES
    Na   22.9898  Na.pbe-spn-kjpaw_psl.0.2.UPF
    Nb   92.9064  Nb.pbe-spn-kjpaw_psl.0.3.0.UPF
    O    15.9994  O.pbe-n-kjpaw_psl.1.0.0.UPF
```

```
ATOMIC_POSITIONS {crystal}
   Na  0.0  0.0  0.0
   Nb  0.5  0.5  0.5
   O   0.5  0.0  0.5
   O   0.0  0.5  0.5
   O   0.5  0.5  0.0

K_POINTS {automatic}
$alat $alat $alat 0 0 0

EOF
  mpirun --oversubscribe -np 4 ~/qe-6.7/bin/pw.x < $sys.scf.in > $sys.scf.out
awk '/!/{print $(NF-1)}' $sys.scf.out >> kpoint
 done
```

Create 3.sh

```
#!/bin/bash
for LA in -0.5 -0.4 -0.3 -0.2 -0.1 0.0 0.1 0.2 0.3 0.4 0.5 ;
#for LAT in 2 4 6 8 10 12 14 16;
do
LAT=`echo $LA | awk '{print($1+7.689)}'`
sys=nanbo3
cat> $sys.scf.in << EOF
&CONTROL
   calculation = 'scf'
```

```
   prefix = 'NaNbO3',
   outdir = './',
   pseudo_dir = '/home/john/PSEUDOPOTENTIALS',
   /
&SYSTEM
   ibrav = 1,
   celldm(1) = $LAT,
   nat = 5,
   ntyp = 3,
   ecutwfc = 75,
   occupations = 'smearing',
   smearing = 'mp',
   degauss = 0.02,
   nspin = 1,
/
&ELECTRONS
   conv_thr = 1.0d-8,
   mixing_beta = 0.7,
   diagonalization = 'david',
/
ATOMIC_SPECIES
   Na   22.9898  Na.pbe-spn-kjpaw_psl.0.2.UPF
   Nb   92.9064  Nb.pbe-spn-kjpaw_psl.0.3.0.UPF
   O    15.9994  O.pbe-n-kjpaw_psl.1.0.0.UPF
```

```
ATOMIC_POSITIONS {crystal}
   Na 0.0  0.0  0.0
   Nb  0.5  0.5  0.5
   O   0.5  0.0  0.5
   O   0.0  0.5  0.5
   O   0.5  0.5  0.0

K_POINTS {automatic}
   6 6 6 0 0 0
EOF
 mpirun --oversubscribe -np 4 ~/qe-6.7/bin/pw.x < $sys.scf.in > $sys.scf.out
awk '/lattice/{alat=$(NF-1)}/!/{print alat, $(NF-1)}' $sys.scf.out >> alat
 done
#ev.x calculation
  ~/qe-6.7/bin/ev.x
```

3.4.3. Density of States (DOS)

The density of states (DOS) is essentially the number of different states at a particular energy level that electrons are allowed to occupy, i.e. the number of electron states per unit volume per unit energy. Bulk properties such as specific heat, paramagnetic susceptibility, and other transport phenomena of conductive solids depend on this function. The density of states is calculated by pseudopotential and plane wave basis set method within the Density Functional Theory (DFT), treating Exchange-Correlation Functional with generalized gradient approximation (GGA) in the form of predew Berke- Erzndof (PBE) functional.

DOS calculations allow one to determine the general distribution of states as a function of energy and can also determine the spacing between energy bands in semi- conductors. Density of states is discontinuous for an interval of energy, which means that no states are available for electrons to occupy within the band gap of the material. This condition also means that an electron at the conduction band edge must lose at least the band gap energy of the material in order to transition to another state in the valence band. The result of the number of states in a band is also useful for predicting the conduction properties.

3.4.4 Post Processing

Stefano Baroni originally developed the package called post processing. They are number of auxiliary codes performing small calculations such as plotting of band, density of States (DOS) etc. The main post processing codes which extract the specified data/files from PWscf calculations and perform further calculations are as follows:

i. **pw.x**: we use this command to run the input files of scf and nscf calculations of energy and wave functions at each and every k-points, which extract the output file for the energy at every k-point. Also, it is use to calculate electronic structure, structural optimization and molecular dynamics.

ii. **ph.x**: This command is used to calculate the phonon frequencies and displacement patterns, dielectric tensors, effective charges (using data produced by pw.x).

iii. **q2r.x**: This code calculates the interatomic force constant (IFC) in real space from dynamic matrices produced by ph.x on a regular q-grid.

iv. **pp.x**: This extract the specified data from file produced by pw.x, prepared data for plotting by writing them into format that can be read by several plotting programs.

v. **matdyn.x**: This code helps in producing phonon frequencies at generic wave vector using IFC file calculated by q2r.x; which may also calculate phonon DOS.

vi. **bands.x**: This extracts the files from PWsef calculations and record its eigenvalues at different k-points with corresponding energies values ready for proper process. The code bands.x also performs the symmetry analysis of the band structure.

vii. **plotband.x**: This code reads the output files of bands.x and then produces band structure for Post Script plots.

viii. **dos.x**: This command is used to calculate the electronic Density of State (DOS) at different k-points.

3.5 BAND STRUCTURE COMPUTATIONAL DETAILS OF $NaNbO_3$

The PWSCF method uses the pw.x and post-processing codes to plot the band structure of $NaNbO_3$. The pw.x code computes the total energy, while PWSCF applies the plane wave pseudopotential approach to perform self-consistent calculations. The procedure follows these steps:

i. Perform a self-consistent calculation (input: nanbo3.scf.in, output: nanbo3.scf.out).

ii. Run a non-self-consistent calculation with more bands (nbnd=10; input: nanbo3.band.in; output: nanbo3.band.out).

iii. Use bands.x to extract eigenvalues and save them to a file (input: nanbo3.bands.in; output: nanbo3.bands.out).

iv. Use plotbands.x to generate a PostScript file (nanbo3bands.ps), which shows the electronic band structure and the band gap.

Before these steps, the kinetic energy cutoff for wave functions (ecutwfc, in Ry) is optimized. The selected ecutwfc is the lowest value that gives the minimum total energy difference. Below are the input pw parameters used for the electronic band structure calculation of $NaNbO_3$.

3.5.1 Elastic Moduli

Elastic moduli (Young's bulk and shear modulus), Zener anisotropic factor, Poisson's ratio are derived from second-order elastic constants. The Zener anisotropic factor can be calculated as

$$\boxed{A = \frac{2C_{44}}{C_{11}-C_{12}}} \quad \text{..... (3.3)}$$

Bulk modulus (B), Shear modulus (G), Poisson's ratio (v), Young modulus (E) were calculated using the following equations;

$$\boxed{B = \frac{C_{11}+2C_{12}}{3}} \quad \text{..... (3.4)}$$

$$G = \frac{c_{11}-c_{12}+3c_{44}}{5} \text{..... (3.5)}$$

$$\boxed{v = \frac{3B-2G}{2(3B+G)}} \quad \text{..... (3.6)}$$

$$\boxed{E = \frac{9BG}{3B+G}} \quad \text{..... (3.7)}$$

CHAPTER FOUR

PRESENTATION AND DISCUSSION OF RESULTS

4.0 STRUCTURAL PROPERTIES:

The studied $NaNbO_3$ perovskite compound crystallizes in the orthorhombic structure with space group Pbnm, where sodium, niobium, and oxygen atoms occupy the distinct lattice positions that define the perovskite framework. The ground-state lattice constant was obtained after full structural optimization, allowing relaxation of both atomic coordinates and lattice parameters. The calculated optimized lattice constants, bulk modulus, pressure derivative, and electronic band gap of $NaNbO_3$ are presented in the table below

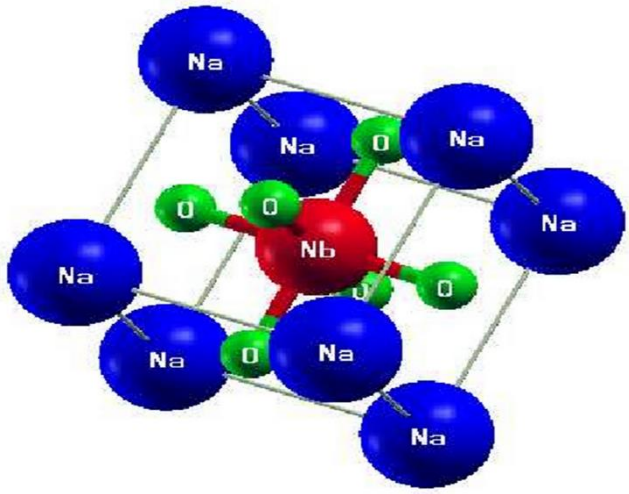

Figure 4.1: Crystallographic structure of $NaNbO_3$ Perovskite compound

4.1 ELECTRONIC PROPERTIES

In the ab-initio analysis of the electronic properties of $NaNbO_3$ perovskite, the band structure and density of states are shown in Figures 4.2 and 4.3. The results reveal a narrow band gap between the conduction and valence bands, confirming its semiconducting nature. For a semiconductor to be suitable for photovoltaic and photocatalytic applications, its band gap should range between 1.4 and 3.0 eV. Based on this range, $NaNbO_3$ is identified as a promising candidate for such applications. The partial density of states (PDOS) analysis shows that the

conduction band is mainly contributed by Nb-4d orbitals, while the valence band is dominated by O-2p orbitals, indicating strong hybridization between Nb and O atoms in the compound.

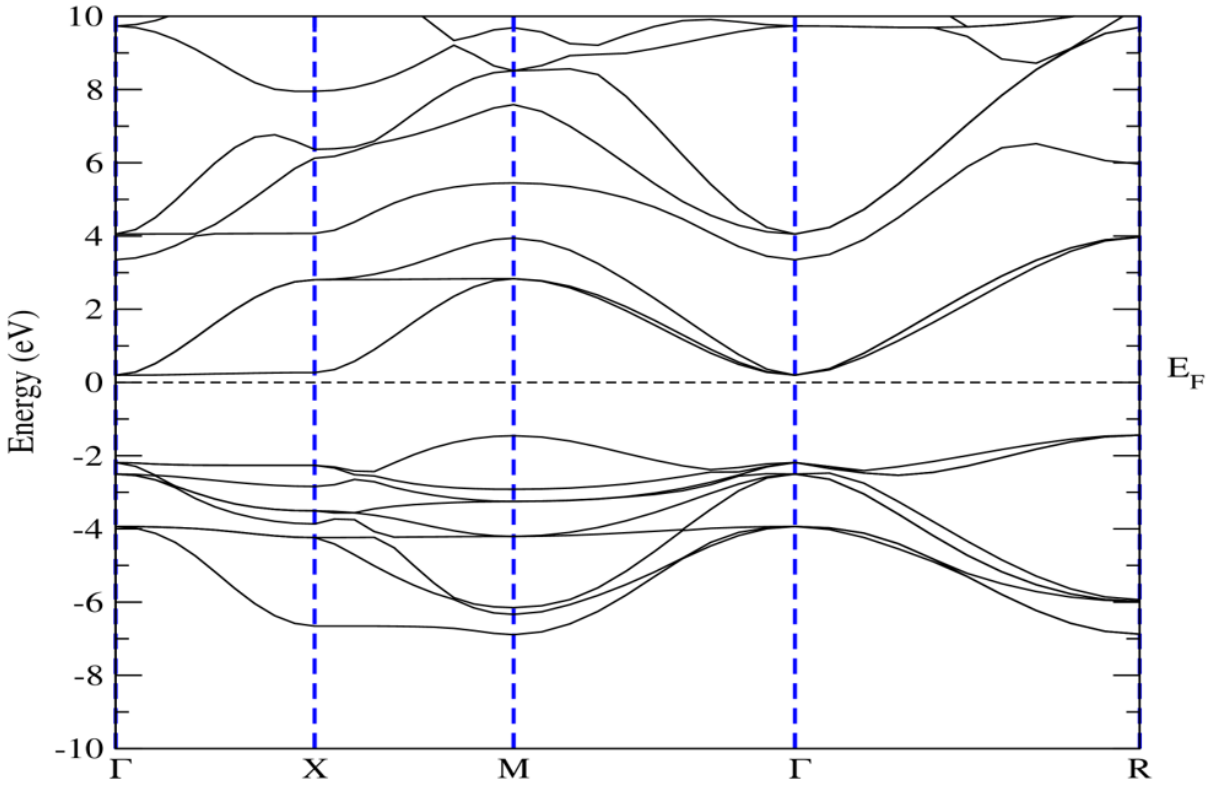

Figure 4.2: $NaNbO_3$ Perovskite compound showing the indirect band gap, confirming it's semiconducting behaviour

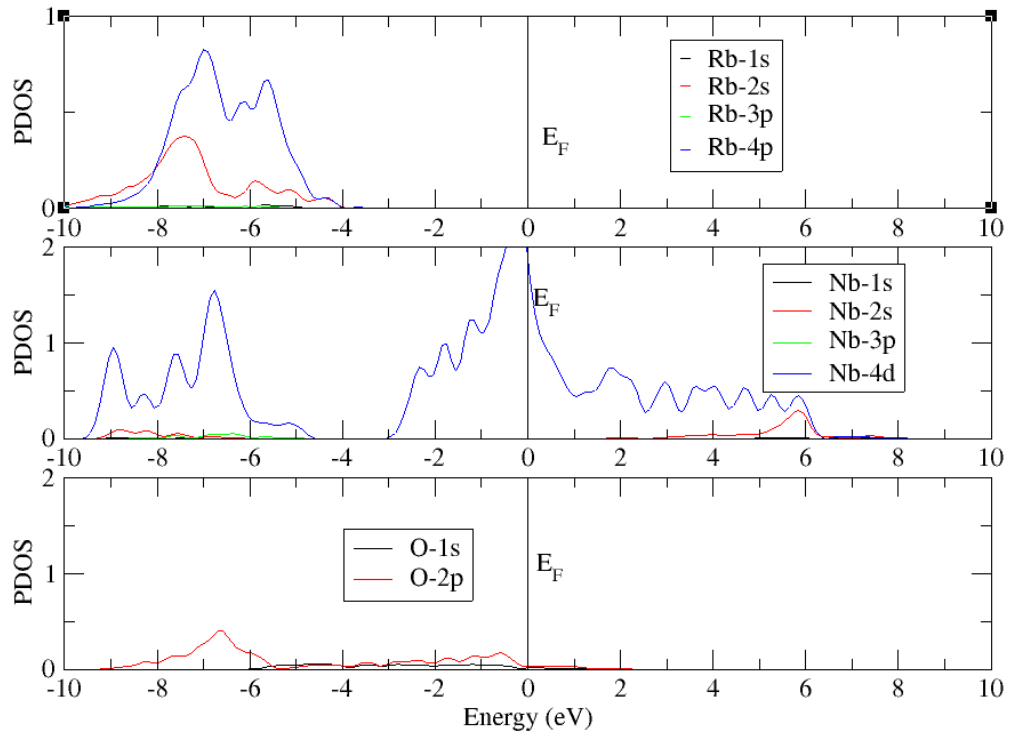

Figure 4.3: Partial density of state of the $NaNbO_3$ Perovskite compound.

As shown in Fig. 4.2, the valence band maximum (VBM) is at the Γ-point and the conduction band minimum (CBM) is at the X-point, confirming an indirect band gap for $NaNbO_3$. The calculated band gap is about 0.4 eV, indicating semiconducting behaviour. The Fermi level lies within the gap, confirming the absence of free charge carriers.

The bands below the Fermi level are mainly from O-2p and Nb-4d states, while the conduction band is dominated by Nb-4d orbitals. The deeper valence bands arise from Na-s and O-p orbitals. This shows that the electronic structure is strongly influenced by the hybridization between Nb-4d and O-2p states.

Charge density distribution suggests that electrons are concentrated around the oxygen and niobium atoms, showing covalent bonding within the Nb–O octahedra. The symmetric band distribution around the Fermi level indicates non-magnetic behavior.

Overall, the band structure and density of states confirm that $NaNbO_3$ is an indirect band gap semiconductor with significant Nb–O interaction governing its electronic properties.

4.3 MECHANICAL PROPERTIES

The mechanical stability of this compound was tested based on the durability of the crystal against external forces, which is a desirable property to ensure its sustainability in any application. The calculated mechanical properties such as elastic constants C_{11}, C_{12}, C_{44}, Young's modulus (E), Shear modulus (G), Bulk modulus (B), Pugh's ratio (B/G), Zener Anisotropic factor (A), Poisson's ratio and Caunchy pressure ($C_p = C_{12} - C_{44}$) are listed in Table 2 below

Table 4.2: showing the elastic constant, Young's modulus (E), Shear modulus (G), Bulk modulus (B), Poisson's ratio (v), Zener Anisotropic factor (A), Pugh's ratio and Caunchy pressure

Mechanical Properties	**Values**
C_{11}(GPa)	**4052.07**
C_{12}(GPa)	**724.77**
C_{44}(GPa)	**741.44**
E(GPa)	**260.383**
G(GPa)	**103.147**
B(GPa)	**183.387**
A	**0.45**
v	**0.26**
C_{12} (GPa) – C_{44} (GPa)	**-16.67**
B/G	**1.78**

The calculated elastic constant values for $NaNbO_3$ satisfy the mechanical stability conditions, confirming that the compound is mechanically stable as shown in Table 4.2. The bulk modulus (B) and shear modulus (G) describe the material's resistance to deformation.

A higher B value indicates stronger resistance to pressure-induced deformation, while a higher G value shows greater resistance to shear stress. The Zener anisotropy factor helps determine whether a material is isotropic or anisotropic. When the factor equals 1, the material is isotropic; when it is greater or less than 1, the material is anisotropic. In this study, the calculated anisotropy factor is 0.798, showing that $NaNbO_3$ is anisotropic in nature. The Pugh ratio (B/G) indicates ductility. If the ratio is above 1.75, the material is ductile; if below, it is brittle. Based on the obtained ratio, $NaNbO_3$ exhibits significant ductile behaviour. As shown in table 4.2, the compound is brittle since its Pugh ratio is less than 1.75. The unidirectional elastic constant (C_{11}) is much higher than C_{44}, showing that $NaNbO_3$ has weaker resistance to pure shear deformation than to unidirectional compression. The Poisson's ratio (ν) describes the bonding forces and compressibility of a material. For most central-force solids, ν ranges between 0.25 and 0.5. The calculated ν values for $NaNbO_3$ fall within this range, indicating that the compound is nearly incompressible and that metallic bonding plays a dominant role in its atomic interactions.

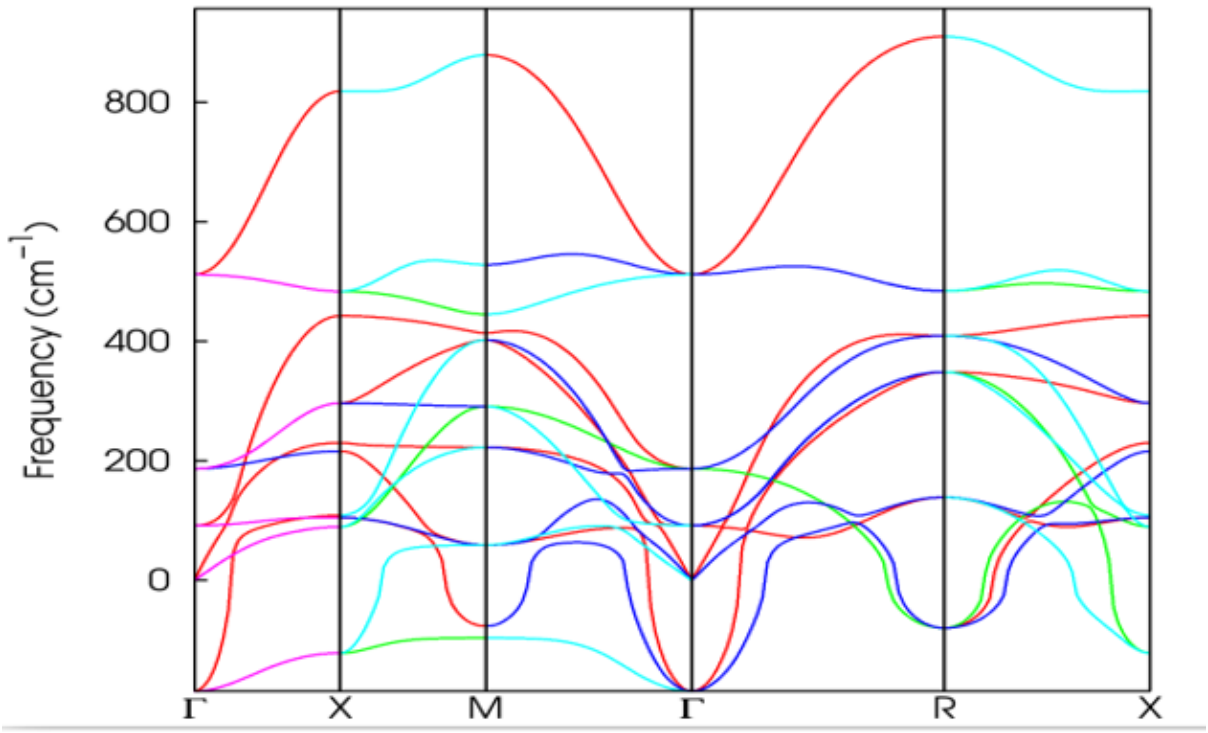

Figure 4.4: Phonon dispersion of $NaNbO_3$ showing lattice vibrations and dynamic instability

CHAPTER FIVE

FINDINGS, CONCLUSION AND SUGGESTIONS FOR FURTHER STUDIES

5.1 FINDINGS

i. The physical properties of $NaNbO_3$ have been studied using first-principles calculations.

ii. The results show that the compound satisfies the mechanical stability conditions.

iii. The band structure indicates that $NaNbO_3$ is an indirect band gap semiconductor, as the valence band maximum and conduction band minimum occur at different symmetry points.

5.2 CONCLUSION

In this theoretical study, the structural, electronic, and mechanical properties of $NaNbO_3$ were investigated using ab-initio density functional theory. The calculated ground state properties show good agreement with reported experimental and theoretical results. The band structure and partial density of states confirm the non-metallic nature of the compound. The optimized lattice parameter (a) also aligns well with available experimental data. The elastic constants and related mechanical parameters, including the bulk modulus (B), shear modulus (G), Young's modulus (E), and Poisson's ratio (ν), were determined. The results confirm that $NaNbO_3$ is mechanically stable according to elastic stability criteria. The electronic band structure shows that $NaNbO_3$ is an indirect band gap semiconductor. The Zener anisotropy factor and Pugh's ratio were also evaluated. The Zener factor indicates that the compound is anisotropic, while the Pugh's ratio value shows that $NaNbO_3$ is brittle in nature.

5.3 SUGGESTIONS FOR FURTHER STUDIES

The first-principles calculations were used to determine the electronic, structural, density of states, and mechanical properties of $NaNbO_3$. It is suggested that further studies should focus on the following properties:

i. Optical properties

ii. Thermoelectric properties

iii. Phonon-lattice properties

REFERENCES

Aksel, E., & Jones, J. L. (2011). Advances in lead-free piezoelectric perovskite materials. *Annual Review of Materials Research, 41*, 305–331.

Babalola, M. I., & Ofomaja, K. A. F. (2024). Spin-resolved DFT studies of a novel ZrFeBi half-Heusler alloy. *Transactions of The Nigerian Association of Mathematical Physics, 19*, 267–274.

Baroni, S., de Gironcoli, S., Dal Corso, A., & Giannozzi, P. (2001). Phonons and related crystal properties from density-functional perturbation theory. *Reviews of Modern Physics, 73*(2), 515–562.

Cavazzoni, C., … & Wentzcovitch, R. M. (2009). Quantum ESPRESSO: A modular and open-source software project for quantum simulations of materials. *Journal of Physics: Condensed Matter*, *21*(39), 395502.

Giannozzi, P., Baseggio, O., Bonfà, P., Brunato, D., Car, R., Carnimeo, I., … & Baroni, S. (2020). Quantum ESPRESSO toward the exascale. *Journal of Chemical Physics, 152*(15), 154105.

Iyorzor, B. E., Babalola, M. I., & Ebuwa, S. O. (2022). Investigating the effect of hydrostatic pressure on the structural, electronic, mechanical, lattice dynamics and optical properties of the cubic perovskite $RbTaO_3$: A DFT approach. *NIPES Journal of Science and Technology Research, 4*(2).

Kim, H. S., Lee, C. W., & Park, N. G. (2005). Perovskite materials for photovoltaic and optoelectronic applications. *Chemical Society Reviews, 44*(19), 5345–5369.

Lebedev, A. I. (2015). First-principles study of the structural and ferroelectric properties of $NaNbO_3$. *Physics of the Solid State, 57*(4), 739–746.

Louie, S. G. (1982)**.** Pseudopotentials in the theory of solids. In M. L. Cohen & J. R. Chelikowsky (Eds.), *Electronic Structure and Optical Properties of Semiconductors.* Springer, Berlin.

Marvin, L., Perdew, J. P., & Wang, Y. (1989). Accurate and simple analytic representation of the electron-gas correlation energy. *Physical Review B, 45*(23), 13244–13249.

Mitchell, R. H. (2002)**.** *Perovskites: Modern and Ancient.* Almaz Press Inc., Thunder Bay, Ontario.

Nelmes, R. J., Kuhs, W. F., & Hewat, A. W. (1980). Structural phase transitions in sodium niobate. *Journal of Physics C: Solid State Physics, 13*(22), 3771–3783.

Perdew, J. P., Burke, K., & Ernzerhof, M. (1996). Generalized gradient approximation made simple. *Physical Review Letters, 77*(18), 3865–3868.

Roni, M. (2018). Catalytic activity and surface chemistry of perovskite-type oxides. *Journal of Catalysis, 361*, 62–72.

Scandolo, S., Giannozzi, P., Cavazzoni, C., de Gironcoli, S., Pasquarello, A., & Baroni, S. (2005). First-principles codes for computational crystallography in the Quantum ESPRESSO package. *Zeitschrift für Kristallographie, 220*(5–6), 574–579.

Sharma, A., & Singh, D. (2019). First-principles study of structural, elastic, and electronic properties of $NaNbO_3$. *Computational Condensed Matter, 20*, e00392.

Yamamoto, T., Kobayashi, M., & Kikegawa, T. (2024)**.** High-pressure phase stability of alkali niobates: A first-principles study. *Journal of Applied Physics, 135*(2), 025901.